GREEN-SYNTHESIZED SILVER NANOPARTICLE-LOADED GUAR GUM/HYDROXYETHYLCELLULOSE SPONGES: PREPARATION, CHARACTERIZATION AND ANTIBACTERIAL ACTIVITY

FILIZ KARA

Baskent University, Faculty of Engineering, Department of Industrial Engineering, Ankara, Türkiye
✉ *Corresponding author: F. Kara, fkara@baskent.edu.tr*

Received July 23, 2026

A natural polymer-based antibacterial sponge system was developed by integrating green-synthesized silver nanoparticles (AgNPs) into a guar gum (GG) and hydroxyethyl cellulose (HEC) matrix. To the best of our knowledge, this is the first study reporting the use of HEC as a green synthesis medium under autoclave-assisted conditions for AgNPs production. Nanoparticle formation was confirmed by UV-Vis spectroscopy, XRD, DLS, and zeta potential analyses. The HEC-AgNPs colloidal solution was directly incorporated into the HEC-GG matrix without isolation or purification steps, followed by citric acid crosslinking and lyophilization to obtain porous sponge structures. The structural and physicochemical properties were characterized by FTIR, TGA, and SEM analyses. Swelling behavior and gel fraction were also evaluated, revealing substantial water uptake and supporting polymer network formation. Antibacterial performance was assessed against *E. coli* and *S. aureus*. This approach, based entirely on natural polymer components, offers a sustainable and practical route for producing porous antibacterial materials.

Keywords: green synthesis, biopolymeric sponge, AgNPs, natural polymer

INTRODUCTION

Cellulose is a naturally occurring polysaccharide widely used in various industrial and scientific fields due to its biodegradable, biocompatible, and renewable nature. However, its limited solubility in water and most solvents restricts its direct application. To overcome these limitations, several cellulose derivatives have been developed, among which hydroxyethyl cellulose (HEC) stands out as a particularly versatile option. HEC is a non-ionic, water-soluble polymer obtained through the modification of cellulose with ethylene oxide. Its structure contains a high number of hydroxyl groups, enabling interactions with various functional groups.[1] These characteristics have led to its widespread use in biotechnology, cosmetic formulations, and industrial applications, including as a thickening agent in food and paint industries, as well as in the design of functional polymer-based materials.[2]

Silver nanoparticles (AgNPs) are among the most effective nanomaterials against a broad range of microorganisms, including multidrug-resistant pathogens, owing to their strong antimicrobial activity. Conventional synthesis methods, however, often rely on toxic chemicals and consume considerable energy, raising environmental and biosafety concerns. For this reason, green synthesis approaches employing plant and microbial extracts, natural polymers, and eco-friendly reducing agents have gained momentum in recent years. Beyond reducing environmental impact, these approaches yield AgNPs with improved biocompatibility and more controllable physicochemical properties.[3] Using natural polymers as reducing and stabilizing agents is especially advantageous, as it limits reliance on toxic reagents while providing a matrix that supports the colloidal stability of the nanoparticles.[4] Among these, HEC has proven to be a useful macromolecular platform for green nanoparticle synthesis. The high density of hydroxyl groups along its backbone offers coordination sites for metal ions, allowing HEC to act as both a reducing and stabilizing agent during nanoparticle formation. This dual functionality facilitates the synthesis of stable AgNPs under mild and environmentally friendly conditions,

while the macromolecular structure of HEC further contributes to their colloidal stability.[5]

Silver nanoparticle-loaded biopolymeric materials have become increasingly relevant for applications requiring antibacterial functionality. Porous and sponge-like natural polymer matrices are particularly well-suited for this purpose, as they can absorb fluids while simultaneously acting as carriers for antibacterial agents.[6] Guar gum (GG) is a biodegradable, non-toxic, water-soluble, and renewable polysaccharide that has gained recognition as a sustainable biopolymer. Its high solubility, effective water retention, and good biocompatibility make it a practical choice for developing functional biopolymeric materials.[7] When combined with cellulose derivatives, such as HEC, guar gum forms hybrid polymer matrices that bring together the complementary properties of each component. Such HEC-GG systems offer a straightforward framework for incorporating antibacterial agents like silver nanoparticles and for producing porous, sponge-like structures with well-defined functional properties.

The present study therefore describes the green synthesis of silver nanoparticles using HEC as both a reducing agent and a synthesis medium under autoclave-assisted conditions. Although HEC has previously been used for AgNPs synthesis under conventional heating conditions, these methods have generally required alkaline conditions,[5,8] whereas its use under autoclave conditions without pH adjustment has not, to the best of our knowledge, been previously reported. The resulting HEC-AgNPs colloidal solution was directly incorporated into a biopolymeric sponge matrix (HEC-GG-based) without an isolation or purification step. This approach, based entirely on natural polymer components, offers a sustainable and practical route for producing porous antibacterial materials. Citric acid crosslinking and lyophilization were applied to obtain the final sponge structures, and their structural, physicochemical, and antibacterial properties were systematically evaluated.

EXPERIMENTAL

Materials

Hydroxyethyl cellulose, guar gum (Sigma-Aldrich), and silver nitrate ($AgNO_3$; ISOLAB Chemicals) were used as raw materials. Anhydrous citric acid, nutrient broth was obtained from Merck (Darmstadt, Germany). The bacterial strains *Staphylococcus aureus* (*S. aureus*) ATCC 25923 and *Escherichia coli* (*E. coli*) ATCC 11229 were obtained from the Biotechnology Laboratory of Gazi University.

Methods

One-pot green synthesis and characterization of AgNPs

AgNPs were synthesized via a green, one-pot autoclave-assisted method, without the use of any additional reducing or toxic chemicals. Briefly, 2 g of HEC was dissolved in 12 mL of deionized water under continuous magnetic stirring until a homogeneous solution was obtained. Subsequently, 12 mL of a 0.4% (w/v) aqueous silver nitrate ($AgNO_3$) solution was slowly added to the HEC solution and stirred at 700 rpm for 5 min to ensure uniform mixing. The resulting mixture was transferred into an autoclave (NÜVE NC 90M), and the synthesis of AgNPs was carried out at 120 °C under 15 psi pressure for 50 min. The formation of AgNPs was preliminarily indicated by a visible color change in the reaction medium after autoclaving, suggesting the reduction of Ag^+ ions and nanoparticle formation.[9,10]

The formation of silver nanoparticles (AgNPs) was monitored using UV-Vis spectroscopy in the wavelength range of 200-800 nm (Digilab Hitachi U-1800, Tokyo, Japan). The hydrodynamic particle size distribution and zeta potential of the AgNPs were determined by dynamic light scattering (DLS) using a Zeta sizer instrument (Malvern Nano ZS90, Malvern Instruments, UK). All measurements were performed at 25 °C with a fixed scattering angle of 173°. The crystalline structure of the AgNPs was analyzed by X-ray diffraction (XRD) using a diffractometer equipped with Cu Kα radiation (MiniFlex, Rigaku Co., Tokyo, Japan), operated over a 2θ range of 0-90°. The morphology and particle size of the AgNPs were examined by scanning electron microscopy (SEM) at an accelerating voltage of 30 kV (Quanta 400F Field Emission, FEI Company, Hillsboro, OR, USA).

Preparation of HEC-GG and AgNPs-loaded sponges

Porous sponges were prepared using HEC, GG, and citric acid (CA) as crosslinking agent. Briefly, 2 g of HEC was dissolved in 30 mL of deionized water under magnetic stirring. Separately, 1 g of GG was dissolved in 30 mL of deionized water. The two solutions were then combined and mixed until a homogeneous solution was obtained. Citric acid was added to the mixture to obtain a final CA concentration of 5% (w/v), and stirring was continued at room temperature.

For AgNPs-loaded sponges, the HEC-AgNPs colloidal solution was incorporated directly into the fabrication process without an intermediate isolation step, minimizing aggregation and simplifying the overall procedure. To keep the total HEC solution volume constant at 30 mL, plain HEC solution was partially replaced with 5, 10, or 15 mL of the HEC-AgNPs colloidal solution, yielding HEC-GG-Ag1, HEC-GG-Ag2, and HEC-GG-Ag3 formulations,

respectively. The theoretical silver concentrations in the final 60 mL HEC-GG mixture were 0.106 mg/mL for HEC-GG-Ag1, 0.212 mg/mL for HEC-GG-Ag2, and 0.318 mg/mL for HEC-GG-Ag3. These values were calculated from the initial $AgNO_3$ amount assuming complete reduction of Ag^+ ions and represent the maximum theoretical silver concentrations, as the actual extent of Ag^+ reduction was not quantitatively determined.

The resulting solutions were poured into molds, frozen, and lyophilized to obtain porous sponge structures. Finally, the dried sponges were thermally treated at 110 °C for 15 min to induce citric acid-mediated crosslinking.

Characterization of sponges

The structural, morphological, and thermal properties of HEC-GG and AgNPs-loaded sponges were characterized using spectroscopic, microscopic, and thermal analysis techniques. Fourier transform infrared spectroscopy (FTIR, Thermo Nicolet iS10 spectrometer, Thermo Fisher Scientific, USA) was employed to identify functional groups and investigate structural changes associated with citric acid-mediated crosslinking. FTIR spectra were recorded in the range of 600-4000 cm^{-1} with 32 scans at a resolution of 4 cm^{-1}.

The morphology and pore structure of the sponges were examined using scanning electron microscopy (SEM; Quanta 400F Field Emission, FEI Company, USA). Prior to imaging, the samples were sputter-coated with a thin layer of gold/palladium to enhance surface conductivity.

Thermal stability and decomposition behavior of the sponges were evaluated by thermogravimetric analysis (TGA; PerkinElmer TGA 4000, USA). The measurements were carried out under a nitrogen atmosphere by heating the samples from 30 °C to 750 °C at a heating rate of 10 °C/min.

Swelling behavior and gel fraction

The swelling behavior and the gel fraction of the sponges were evaluated gravimetrically. Pre-weighed dry sponge samples (W_0) were immersed in phosphate-buffered saline (PBS) at room temperature. At predetermined intervals (1, 2, 3, and 24 h), the samples were removed from PBS, gently blotted with absorbent paper to remove excess surface liquid, and immediately weighed (W_t). The swelling ratio (SR) was calculated using Equation (1):

$$SR\ (\%) = [(W_t - W_0) / W_0] \times 100 \quad (1)$$

After 24 h of immersion, the samples were rinsed with distilled water, dried in an oven at 40 °C for 24 h, and weighed again (W_d). The gel fraction (GF), expressed as the percentage of dry mass retained after immersion and washing, was calculated using Equation (2):

$$GF\ (\%) = (W_d / W_0) \times 100 \quad (2)$$

All measurements were performed in triplicate, and the results are expressed as mean ± standard deviation.

Antibacterial activity of sponges

The antimicrobial activity of the HEC-GG and AgNPs-loaded sponges was evaluated using the disk diffusion method against Gram-positive *S. aureus* and Gram-negative *E. coli*. Bacterial strains were cultured in nutrient broth at 37 °C for 16-18 h to obtain fresh, active cultures. The turbidity of each culture was adjusted to the 0.5 McFarland standard, corresponding to approximately 1.5×10^8 CFU/mL.

A 100 µL aliquot of the standardized bacterial suspension was uniformly spread onto Mueller-Hinton agar plates using a sterile Drigalski spatula. Sterile sponge discs were then placed onto the inoculated agar surface, and the plates were incubated at 37 °C for 24 h. Following incubation, the diameters of the inhibition zones formed around the samples were measured using a digital caliper.[11] All measurements were performed in duplicate, and the average inhibition zone diameter was reported for each formulation.

RESULTS AND DISCUSSION

AgNPs Characterization

UV-Vis spectroscopy analysis

The formation of silver nanoparticles was monitored by UV-Vis spectroscopy, and the corresponding absorption spectra are presented in Figure 1a. The initially colorless HEC solution gradually turned dark brown upon completion of the reaction, providing a preliminary visual indication of AgNPs formation. As shown in Figure 1a, the UV-Vis spectrum displays a distinct absorption band centered at approximately 445 nm, which is attributed to the surface plasmon resonance (SPR) of silver nanoparticles. This SPR band, typically observed in the 400-500 nm range for AgNPs, confirms the successful reduction of Ag^+ ions to metallic Ag^o and the formation of nanoparticles.[12] Moreover, previous studies have reported that SPR peaks appearing between 410 and 450 nm are characteristic of predominantly spherical AgNPs, suggesting that the synthesized nanoparticles may have a similar morphology.[13] The position and shape of the SPR band can be influenced by synthesis conditions, including polymer concentration, reaction temperature, and time, as well as the resulting nanoparticle size and size distribution.[5,14] The weak shoulder observed at approximately 350-360 nm may be associated with an additional plasmon resonance contribution, as similar features have been reported for silver nanostructures and biopolymer-mediated AgNPs.[15,16]

DLS and zeta potential analysis

The average particle size, polydispersity index (PDI), and zeta potential of the green-synthesized AgNPs were determined using a Nano Zeta sizer instrument. Particle size and PDI measurements were carried out by DLS. As shown in Figure 1b, the AgNPs exhibited an average hydrodynamic particle size of 102.6 nm with a PDI value of 0.235, indicating a relatively narrow particle size distribution. The polydispersity index (PDI) is a parameter describing the heterogeneity of particle sizes within a colloidal system and ranges from 0 to 1, where lower values correspond to more uniform particle distributions.[17] Zeta potential measurements revealed a surface charge of −2.35 mV for the AgNPs (Fig. 1c). Zeta potential is commonly used to assess electrostatic interactions between nanoparticles, and values greater than +30 mV or less than −30 mV are generally associated with strong electrostatic repulsion.[18] The relatively low zeta potential value obtained in this study suggests limited electrostatic repulsive forces between the nanoparticles. However, in green synthesis systems, polymeric materials such as HEC can adsorb onto the nanoparticle surface and form a steric barrier, which may restrict particle-particle interactions and reduce the tendency toward agglomeration even at low zeta potential values.[19] Accordingly, the observed particle size distribution is attributed to steric effects induced by the HEC coating rather than electrostatic repulsion.

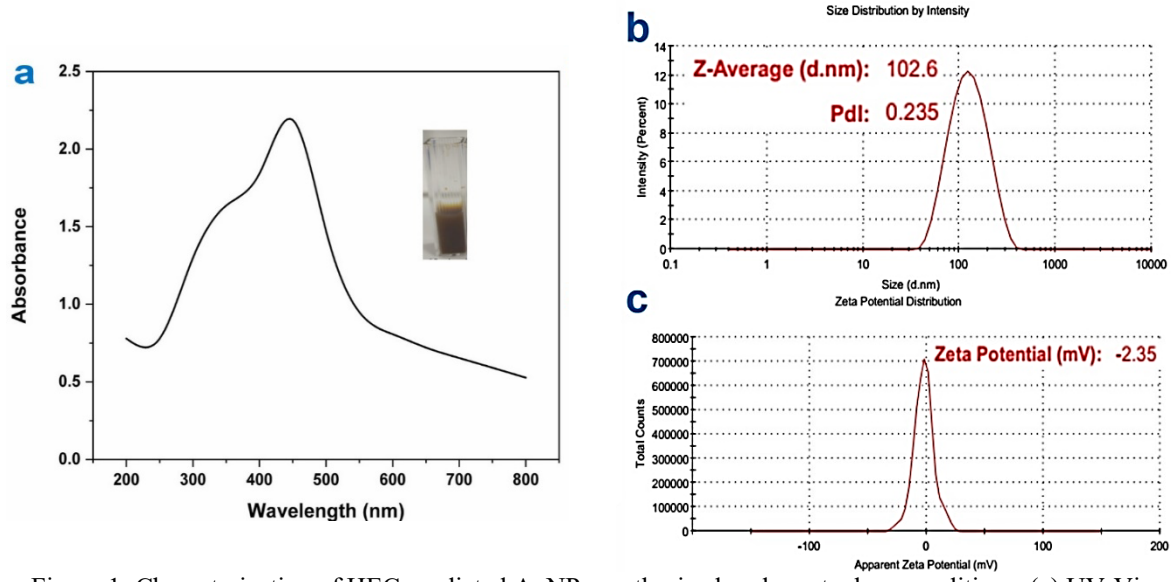


Figure 1: Characterization of HEC-mediated AgNPs synthesized under autoclave conditions: (a) UV-Vis absorption spectrum, (b) DLS particle size distribution, and (c) zeta potential analysis

FTIR analysis

The FTIR spectra of HEC and HEC-mediated AgNPs synthesized under autoclave conditions were comparatively evaluated to investigate the possible involvement of HEC functional groups during nanoparticle formation and given in Figure 2. In the spectrum of HEC, the broad absorption band observed at approximately 3300 cm^{-1} was attributed to O-H stretching vibrations associated with the extensive intermolecular and intramolecular hydrogen bonding of the polysaccharide structure. The band located around 2870 cm^{-1} corresponded to aliphatic C-H stretching vibrations in the HEC structure. In addition, the bands observed in the 1360-1420 cm^{-1} region were attributed to C-H and O-H bending vibrations. The characteristic peaks detected in the 1020-1150 cm^{-1} region was assigned to glycosidic C-O-C and C-O stretching vibrations, confirming the characteristic polysaccharide backbone of HEC.[20,21]

Following autoclave-assisted AgNPs synthesis, noticeable changes were observed in several characteristic HEC bands. The broad O-H stretching band shifted from 3279 to 3312 cm^{-1} and showed a reduction in intensity, suggesting changes in the hydrogen-bonding environment after nanoparticle formation. Similarly, the band at 1418 cm^{-1} shifted to approximately 1402 cm^{-1}, while the characteristic C-O/C-O-C stretching vibration shifted from 1053 to 1044 cm^{-1} in the HEC-AgNPs spectrum. These spectral changes may indicate interactions between hydroxyl- and oxygen-containing groups of HEC and the AgNPs surface during the autoclave process. Similar changes in HEC functional groups have also been

reported for HEC-mediated AgNPs synthesized under conventional heating conditions, supporting the involvement of HEC functional groups in Ag^+ reduction and nanoparticle stabilization.[5] The main polysaccharide bands remained preserved after synthesis, indicating that the primary HEC backbone structure was largely maintained. Overall, the FTIR findings suggest that HEC may contribute not only to the formation of AgNPs, but also to their stabilization within the polymeric matrix.

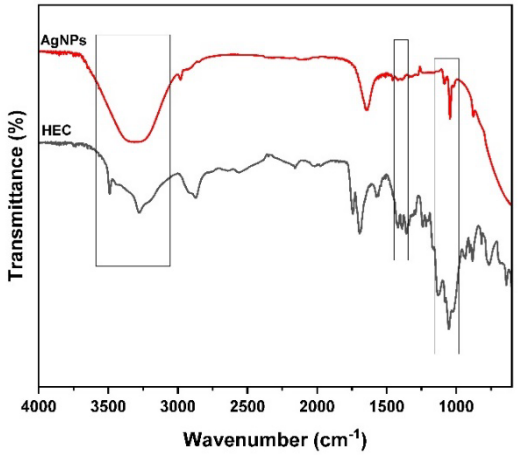


Figure 2: FTIR spectra of HEC and HEC-mediated AgNPs synthesized under autoclave conditions

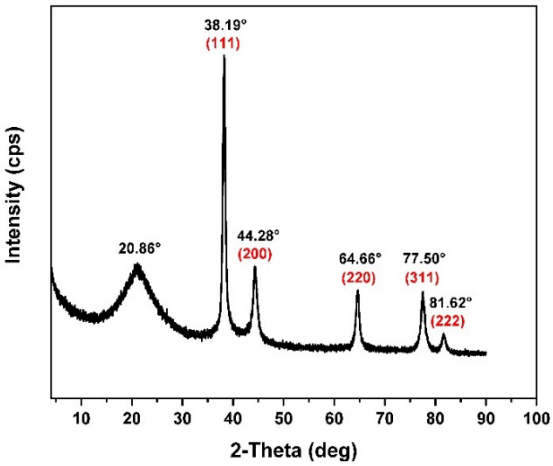


Figure 3: XRD pattern of HEC-mediated AgNPs synthesized under autoclave conditions, showing the characteristic diffraction peaks of crystalline AgNPs

XRD analysis

The crystalline structure and phase composition of the synthesized nanoparticles were analyzed by X-ray diffraction (XRD), and the corresponding diffraction pattern is presented in Figure 3. The diffractogram showed peaks at 2θ values of 20.86°, 38.19°, 44.28°, 64.66°, 77.50°, and 81.62°. The broad diffraction peak observed at 20.86° is attributed to hydroxyethyl cellulose (HEC) present in the synthesis medium. Polysaccharides generally exhibit limited crystallinity because their high molecular weight and branched molecular architecture hinder the regular packing of polymer chains within an ordered crystal lattice.[22] As a result, these materials typically display predominantly amorphous or semi-crystalline structures, which is reflected in the broad peak associated with HEC.

The diffraction peaks at 38.19°, 44.28°, 64.66°, 77.50°, and 81.62° correspond to the (111), (200), (220), (311), and (222) crystallographic planes of metallic silver. These reflections are characteristic of the face-centered cubic (FCC) structure of silver and agree well with the standard diffraction data reported for metallic Ag.[23] The intensity and sharpness of these peaks indicate the crystalline nature of the synthesized Ag nanoparticles. In addition, no diffraction peaks related to impurity phases or silver oxide were detected. This observation suggests that the synthesized nanoparticles consist predominantly of metallic silver. The presence of well-defined Ag reflections also indicates that HEC acted as a stabilizing polymer during synthesis without altering the crystalline structure of the silver nanoparticles.

Characterization of sponges

FTIR analysis

The FTIR spectra of HEC, GG, and HEC-GG sponge samples are presented in Figure 4a, while the spectra of AgNPs-loaded sponge samples are shown in Figure 4b. The characteristic FTIR bands of HEC were discussed in the previous section; therefore, only the main comparative changes observed after sponge formation and AgNPs incorporation are highlighted here. The FTIR spectrum of GG exhibited absorption bands largely similar to those of HEC due to the polysaccharide nature of both polymers (Fig. 4a). A broad band observed around 3278 cm^{-1} was attributed to O-H stretching vibrations associated with hydroxyl groups and intermolecular hydrogen bonding, while the band near 2925 cm^{-1} corresponded to aliphatic C-H stretching vibrations. The absorption bands detected at approximately 1418, 1388, and 1360 cm^{-1} were associated with C-H and O-H bending vibrations of the polysaccharide backbone. In the fingerprint region, the

characteristic bands observed between 1056 and 1139 cm^{-1} were assigned to glycosidic C-O-C and C-O stretching vibrations of the GG polysaccharide structure. In addition, bands observed around 1171 cm^{-1} and within the 766-944 cm^{-1} region reflected contributions from the fingerprint region of the guar gum structure.[24] Compared with the spectra of the individual polymers, the HEC-GG sponge spectrum retained the main characteristic polysaccharide bands, indicating that the backbone structures of both HEC and GG were largely preserved after sponge formation (Fig. 4a). However, noticeable changes were observed in the O-H stretching region (3280-3490 cm^{-1}) and in the glycosidic C-O-C vibration region (1056-1216 cm^{-1}).[25] These spectral variations may be associated with intermolecular interactions between HEC, GG, and citric acid during sponge formation. Since both polymers contain abundant hydroxyl and ether groups, the observed changes are likely related to modifications in the hydrogen-bonding environment and the formation of a more integrated polymeric network. A weak absorption in the 1720-1730 cm^{-1} region was also observed in the sponge spectrum. However, this band was not considered direct evidence of newly formed ester linkages. Similar absorptions were also observed in the spectra of the individual HEC and GG components, possibly arising from residual carbonyl-containing groups and/or overlapping absorbed water vibrations commonly observed in polysaccharide systems. Furthermore, no significant shift in band position was observed between the individual components and the sponge spectrum, which would otherwise be expected upon formation of new ester bonds. Therefore, the FTIR findings mainly support the formation of a physically integrated and possibly partially crosslinked HEC-GG network rather than extensive covalent modification.[26]

The FTIR spectra of AgNPs-loaded HEC-GG sponge samples (Fig. 4b) remained largely similar to that of the HEC-GG sponge. The broad O-H stretching band was still centered around 3280-3290 cm^{-1}, while the characteristic glycosidic C-O-C and C-O stretching vibrations remained detectable near 1139, 1081, and 1052 cm^{-1} in all AgNPs-containing sponge formulations. Likewise, the bands located in the 1358-1418 cm^{-1} region remained at nearly identical positions after AgNPs incorporation. No distinct new absorption bands or major peak shifts were observed with increasing AgNPs content. The preservation of the main polysaccharide absorption bands indicates that AgNPs incorporation did not substantially alter the chemical structure of the HEC-GG sponge matrix. Since metallic AgNPs do not exhibit characteristic absorption bands in the mid-IR region, the absence of new FTIR bands after AgNPs incorporation is expected.[27] The slight attenuation of O-H and glycosidic C-O-C band intensities observed in AgNPs-loaded sponges compared to the unloaded sponge may reflect physical interactions between the nanoparticle surface and the hydroxyl or ether oxygen groups of the polymer matrix. AgNPs incorporation generally preserves the main polysaccharide FTIR bands, while only minor spectral variations may occur due to physical interactions between nanoparticles and hydroxyl or oxygen containing groups of the polymer matrix.

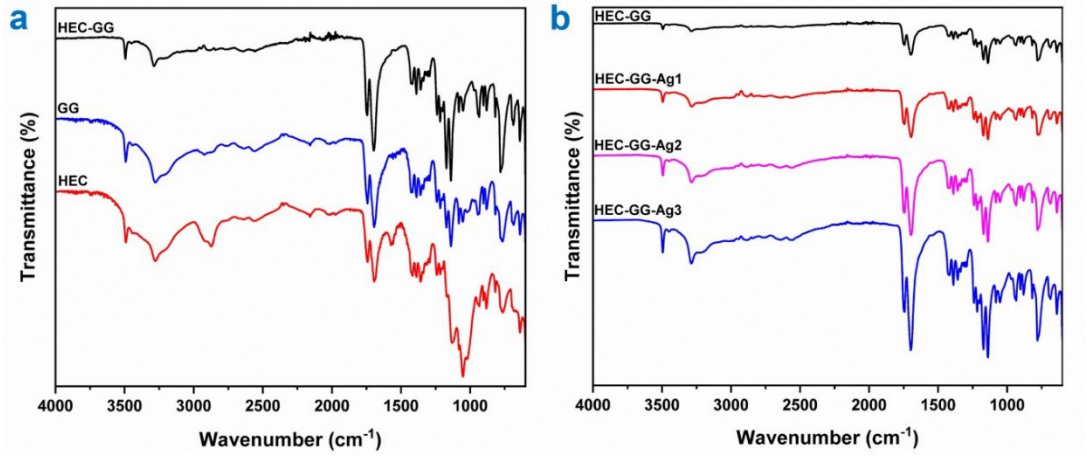


Figure 4: FTIR spectra of (a) HEC, GG, and HEC-GG sponge samples, and (b) AgNPs-loaded HEC-GG sponge samples

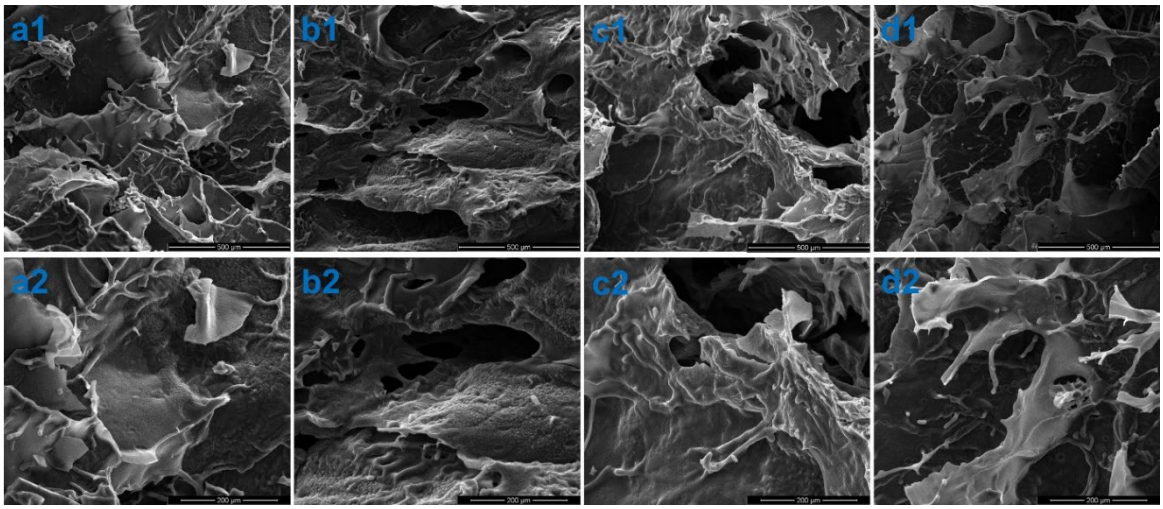


Figure 5: SEM images of sponge samples (a) HEC-GG, (b) HEC-GG-Ag1, (c) HEC-GG-Ag2, and (d) HEC-GG-Ag3 shown at two magnifications (a1-d1) 500 µm and (a2-d2) 200 µm scale bar

Therefore, the present FTIR findings mainly suggest that AgNPs were incorporated into the sponge network, without causing substantial modification of the primary HEC-GG polysaccharide backbone.[5]

SEM analysis

The morphological properties of the sponges were examined by SEM analysis, and the obtained images are presented in Figure 5. All sponge samples displayed a highly porous, interconnected network structure, which is characteristic of freeze-dried polymer matrices. The Ag-free sponge (HEC-GG, a1-a2) showed relatively smooth and thin pore walls with an open, irregular pore arrangement. In HEC-GG-Ag1 (b1-b2), the pore walls appeared slightly thicker, while the general porous structure was preserved. HEC-GG-Ag2 (c1-c2) showed a more irregular pore wall morphology with visible surface heterogeneity. At the highest AgNPs loading, HEC-GG-Ag3 (d1-d2) exhibited the roughest pore wall surfaces among all samples. At higher magnification (a2-d2), the AgNPs-loaded sponges showed a granular surface texture and occasional nodular features on the pore walls, which were absent in the Ag-free control. Overall, increasing AgNPs content appeared to influence both the surface texture and pore wall morphology of the sponge network.

TGA-DTG analysis

The thermal behavior of the HEC-GG sponge and the AgNPs-loaded sponges (HEC-GG-Ag1, HEC-GG-Ag2, and HEC-GG-Ag3) was examined by TGA and DTG (Fig. 6a and 6b). All samples lost weight in more than one step, as expected for a matrix made from two polysaccharides and a citric acid crosslinker. The first weight loss, below about 150 °C, was small (around 4-6 wt%) and is linked to the release of adsorbed and hydrogen-bonded water held within the porous polysaccharide matrix.[28,29] The HEC-GG-Ag samples lost slightly less water in this region than the HEC-GG sponge, which may reflect interactions between the nanoparticle surface and the hydroxyl groups of the polymers that reduce the number of free sites available to bind water. The main weight loss occurred between about 180 and 260 °C, where the sharpest DTG minimum was recorded. For the HEC-GG sponge, this minimum was centered near 207 °C and corresponds to the main breakdown of the polysaccharide backbone, involving cleavage of glycosidic bonds and the citric acid ester crosslinks, together with dehydration and depolymerization of the guar gum and HEC chains.[28] A second, weaker DTG feature appeared near 355-360 °C in all samples and reflects the further oxidation and carbonization of the remaining organic fragments.[28] The addition of AgNPs caused only minor changes in the degradation profile. In the HEC-GG-Ag samples, the rate of the main decomposition step, seen as the depth of the DTG peak, was somewhat lower than in the HEC-GG sponge, which points to a slightly slower breakdown of the polymer chains. This can be linked to local interactions between the silver species and the surrounding polymer network, as reported for other silver-polymer systems.[30] The most noticeable difference was in the residue left at 700 °C. The HEC-GG sponge retained about 5-

6 wt%, while the HEC-GG-Ag samples retained close to 9 wt%. Since metallic silver remains thermally stable at these temperatures, this higher residue is consistent with the presence of inorganic silver in the sponges and provides indirect evidence for successful AgNPs incorporation.[30] Overall, AgNPs incorporation slightly modifies the thermal decomposition of the HEC-GG sponges and offers a small improvement in thermal resistance, while the basic multi-step degradation pattern of the polysaccharide structure is preserved.

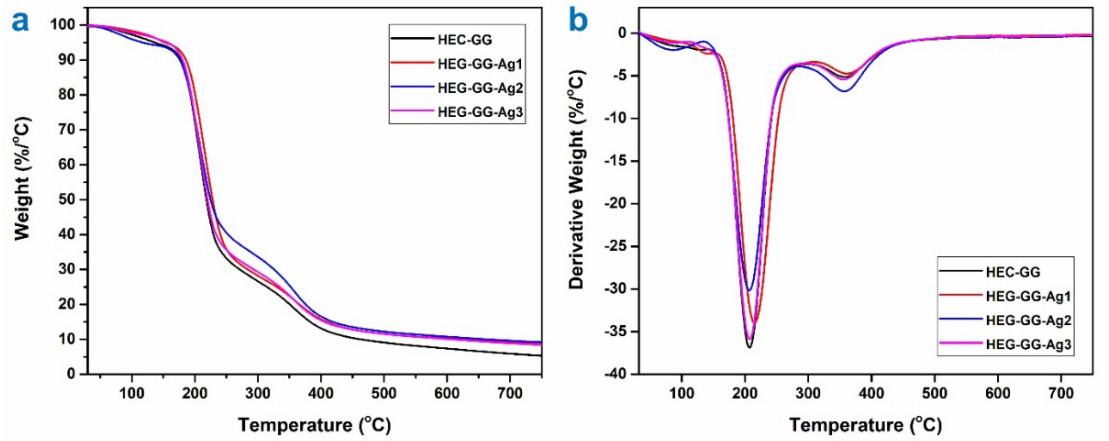


Figure 6: TGA (a) and DTG (b) curves of HEC-GG and AgNPs-loaded sponges

Table 1
Swelling ratio (SR) and gel fraction (GF) of HEC-GG and AgNPs-loaded sponges in PBS at room temperature

Sample	SR 1 h (%)	SR 2 h (%)	SR 3 h (%)	SR 24 h (%)	GF (%)
HEC-GG	568 ± 89	733 ± 57	640 ± 42	350 ± 62	59.2 ± 1.9
HEC-GG-Ag1	830 ± 191	745 ± 190	637 ± 150	426 ± 143	82.8 ± 1.0
HEC-GG-Ag2	780 ± 118	788 ± 78	717 ± 96	443 ± 127	85.5 ± 6.2
HEC-GG-Ag3	756 ± 52	782 ± 81	709 ± 132	479 ± 119	65.4 ± 1.6

Gel fraction

The gel fraction values of HEC-GG, HEC-GG-Ag1, HEC-GG-Ag2, and HEC-GG-Ag3 were 59.2%, 82.8%, 85.5%, and 65.4%, respectively (Table 1). All sponges retained a substantial proportion of their initial dry mass after 24 h in PBS and subsequent washing. The AgNPs-loaded sponges showed higher gel fraction values than the HEC-GG control, but no clear trend was observed with increasing AgNPs content.

The retention of an insoluble fraction provides evidence of polymer network formation during thermal treatment with citric acid. Similar network formation has been reported for citric acid-crosslinked cellulose-based hydrogels.[31] In the present study, approximately 15-41% of the initial dry mass was lost during immersion and washing, possibly due to the removal of uncrosslinked polymer chains and other soluble components. Overall, the gel fraction results support the formation of a stable polymer network in the prepared sponges.

Swelling behavior

The swelling ratios of the sponges in PBS are presented in Table 1. All formulations showed substantial swelling during the first 2 h of immersion. At 2 h, the swelling ratios were 733%, 745%, 788%, and 782% for HEC-GG, HEC-GG-Ag1, HEC-GG-Ag2, and HEC-GG-Ag3, respectively. The AgNPs-loaded sponges showed slightly higher mean swelling ratios than the HEC-GG control at this time point, although no consistent trend was observed with increasing AgNPs content. The swelling ratios were lower after 24 h for all formulations.

The high swelling ratios can be attributed to the hydrophilic nature of HEC and GG, whose hydroxyl groups interact with water, and the porous structure of the freeze-dried sponges, which facilitates liquid penetration. The water uptake of

citric acid-crosslinked cellulose-based hydrogels has likewise been attributed to the hydrophilic hydroxyl groups of the polymer chains.[31] The lower swelling ratios after 24 h may be partly related to the loss of soluble components during immersion, as suggested by the gel fraction results. However, because the swelling ratios were calculated relative to the initial dry mass, this decrease does not necessarily indicate reduced water uptake by the remaining insoluble network.

Antibacterial activity

To evaluate the antibacterial performance of the HEC-GG sponge samples, a disk diffusion assay was performed against *S. aureus* and E. coli (Fig. 7). The resulting inhibition zone diameters are given in Table 2. The AgNPs-free HEC-GG sponge showed no inhibition against *E. coli*, and a small zone (0.75 mm) against *S. aureus*. This confirms that the sponge matrix alone has no meaningful antibacterial effect. Once AgNPs were added, clear inhibition zones appeared for both bacteria. The zone size tended to increase with higher AgNPs content, reaching about 2.00 mm for *S. aureus* and 1.75 mm for *E. coli* at the highest loading (HEC-GG-Ag3). This suggests a dose-related antibacterial effect.

This result is consistent with the known antibacterial mechanisms of AgNPs. These include damaging the bacterial cell membrane, generating reactive oxygen species, denaturing proteins, inhibiting enzymes, and releasing Ag^+ ions that interfere with DNA replication and other cell functions.[32] As more AgNPs are loaded into the sponge, more active silver becomes available to act against bacteria. Since the HEC-AgNPs colloidal solution was incorporated into the sponges without purification, residual Ag^+ ions may also be present in the matrix and contribute to the observed antibacterial activity.

At all AgNPs loadings, the sponges were more effective against *S. aureus* than against *E. coli*. This is usually explained by differences in the cell envelope of Gram-positive and Gram-negative bacteria. *S. aureus* does not have an outer membrane, so silver species can reach its cell surface more easily. *E. coli*, on the other hand, has an outer membrane containing lipopolysaccharides, which acts as an extra barrier and slows down the entry of AgNPs and Ag^+ ions. This likely explains why *E. coli* was less sensitive.[33,34]

Although inhibition increased with AgNPs loading, the zones remained small overall. This is typical for sponge-type materials, where most of the loaded AgNPs are expected to stay trapped inside the porous structure. This possibility is broadly supported by FTIR results, which showed a slight attenuation of O-H and glycosidic C-O-C band intensities in the AgNPs-loaded sponges, which may reflect physical interactions between the AgNPs surface and the hydroxyl/ether oxygen groups of the polymer matrix. Such interactions could contribute to limiting AgNPs mobility within the network, consistent with the idea that only a small, diffusible fraction of silver reaches the agar. Accordingly, the disk diffusion results are likely to mainly reflect the silver released from the sponge, rather than the total silver content of the material.[35,36]

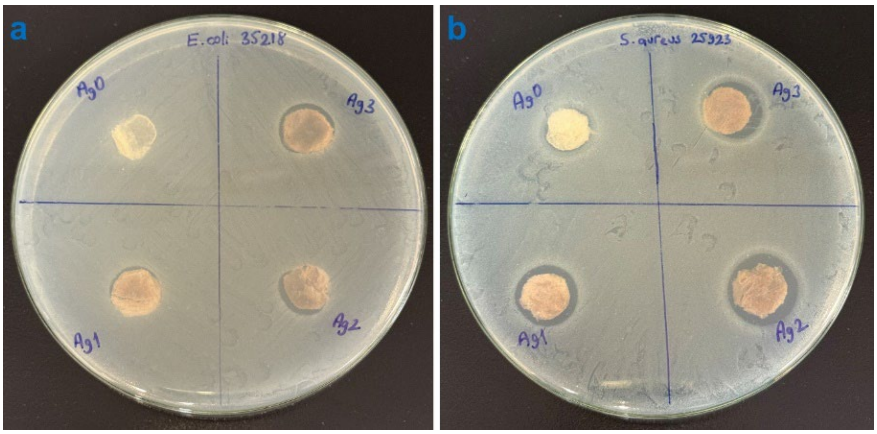


Figure 7: Disk diffusion test results of HEC-GG and AgNPs-loaded HEC-GG sponge samples against *S. aureus* and *E. coli*

Table 2
Measured inhibition zone diameters (mm) for HEC-GG and AgNPs-loaded HEC-GG sponge samples against *S. aureus* and *E. coli*

Sample	*S. aureus* (mm)	*E. coli* (mm)
HEC-GG	0.75± 0.25	-
HEC-GG-Ag1	1.50± 0.00	0.50 ± 0.00
HEC-GG-Ag2	1.75 ± 0.25	0.50 ± 0.00
HEC-GG-Ag3	2.00 ± 0.00	1.75 ± 0.25

CONCLUSION

In this study, silver nanoparticles were successfully synthesized using hydroxyethyl cellulose as both a reducing and stabilizing agent under autoclave-assisted conditions. To the best of our knowledge, this is the first study reporting the use of HEC as both a reducing and stabilizing polymer for AgNPs synthesis under autoclave conditions without external pH adjustment. UV-Vis spectroscopy confirmed nanoparticle formation through a characteristic SPR band at approximately 445 nm, and XRD analysis verified the face-centered cubic crystalline structure of metallic silver, with no detectable impurity phases. DLS measurements yielded an average hydrodynamic size of 102.6 nm, with a narrow size distribution. Despite the low zeta potential value, the colloidal stability of the nanoparticles was attributed to steric effects of the HEC coating surrounding the nanoparticle surface. The HEC-AgNPs colloidal solution was incorporated directly into HEC-GG-based matrices, without an intermediate isolation step, which simplified fabrication and reduced the risk of aggregation. Porous sponges were then obtained by citric acid crosslinking and lyophilization. FTIR analysis showed that the polysaccharide backbone of both HEC and GG remained intact after sponge formation and AgNPs incorporation. SEM images revealed a porous, interconnected network in all samples, with pore wall morphology showing visible changes upon AgNPs incorporation. The sponges also exhibited substantial swelling in PBS, while the gel fraction results supported polymer network formation during citric acid-mediated thermal treatment. TGA showed that AgNPs-loaded sponges left more residue at 700 °C than the Ag-free control, which is expected since metallic silver does not decompose at these temperatures and points to successful nanoparticle incorporation. Disk diffusion tests showed clear antibacterial activity against both *S. aureus* and *E. coli* once AgNPs were added, and inhibition zones grew larger with increasing AgNPs content. *S. aureus* was more sensitive than *E. coli* at all loadings, likely because the outer membrane of *E. coli* presents an additional barrier against silver species. In summary, HEC played a dual role in this work: it served as the synthesis medium for AgNPs production and as a matrix component in the final sponge structure. This allowed the entire process to be carried out without isolating the nanoparticles at any stage, resulting in a simple and waste-minimizing fabrication route for porous antibacterial biopolymeric sponges. Since the HEC-AgNPs colloidal solution was incorporated without purification and the sponges were not washed, the presence of residual Ag^+ ions cannot be excluded. Therefore, quantitative evaluation of residual ionic silver, silver release behavior, and cytotoxicity is necessary before the suitability of these materials for biomedical applications can be established.

REFERENCES

[1] W. Wang, J. Wang, Y. Kang and A. Wang, *Compos. B Eng.*, **42**, 809 (2011), https://doi.org/10.1016/j.compositesb.2011.01.018
[2] A. Al-Mamari, F. Shahitha, M. Al-Sibani, A. Al Saadi, A. Al Harrasi *et al.*, *Lett. Appl. NanoBioSci.*, **12**, 069 (2023), https://doi.org/10.33263/LIANBS123.069
[3] M. Madhusudanan, J. Zhang, S. Pandit, P. Singh, G. J. Jeong *et al.*, *Adv. Nanobiomed. Res.*, **5**, 2400194 (2025), https://doi.org/10.1002/anbr.202400194
[4] V. K. Sharma, R. A. Yngard and Y. Lin, *Adv. Colloid Interface Sci.*, **145**, 83 (2009), https://doi.org/10.1016/j.cis.2008.09.002
[5] M. A. El-Sheikh, S. M. El-Rafie, E. S. Abdel-Halim and M. H. El-Rafie, *J. Polym.*, **2013**, 650837 (2013), https://doi.org/10.1155/2013/650837
[6] K. Boonpavanitchakul, N. Pimpha, W. Kangwansupamonkon and R. Magaraphan, *Eur. Polym. J.*, **130**, 109649 (2020), https://doi.org/10.1016/j.eurpolymj.2020.109649
[7] A. Zarbab, A. Sajjad, A. Rasul, F. Jabeen and M. Javaid Iqbal, *Saudi J. Biol. Sci.*, **30**, 103731 (2023), https://doi.org/10.1016/j.sjbs.2023.103731
[8] T. Suwan, S. Khongkhunthian and S. Okonogi, *Drug Discov. Ther.*, **13**, 70 (2019), https://doi.org/10.5582/ddt.2019.01021

[9] M. Venkatesham, D. Ayodhya, A. Madhusudhan, N. Veera Babu and G. Veerabhadram, *Appl. Nanosci.*, **4**, 113 (2014), https://doi.org/10.1007/s13204-012-0180-y
[10] J. Wongpreecha, D. Polpanich, T. Suteewong, C. Kaewsaneha and P. Tangboriboonrat, *Carbohyd. Polym.*, **199**, 641 (2018), https://doi.org/10.1016/j.carbpol.2018.07.039
[11] C. H. Collins, P. M. Lyne and J. M. Grange, "Collins and Lyne's Microbiological Methods", 7th ed., Butterworth-Heinemann, 1995
[12] J. M. Ashraf, M. A. Ansari, H. M. Khan, M. A. Alzohairy and I. Choi, *Sci. Rep.*, **6**, 20414 (2016), https://doi.org/10.1038/srep20414
[13] Z. Zaheer and Rafiuddin, *Colloids Surf. B Biointerfaces*, **90**, 48 (2012), https://doi.org/10.1016/j.colsurfb.2011.09.037
[14] F. Kara, *Gazi University Journal of Science Faculty*, **5**, 169 (2024), https://dergipark.org.tr/tr/pub/guffd/issue/88281/1536864
[15] R. Kozioł, M. Łapiński, P. Syty, D. Koszelow, W. Sadowski *et al.*, *Beilstein J. Nanotechnol.*, **11**, 494 (2020), https://doi.org/10.3762/bjnano.11.40
[16] H. I. Salaheldin, M. H. K. Almalki and G. E. H. Osman, *IET Nanobiotechnol.*, **11**, 420 (2017), https://doi.org/10.1049/iet-nbt.2016.0126
[17] Y. Wang and S. Wei, *ACS Omega*, **7**, 1494 (2022), https://doi.org/10.1021/acsomega.1c06267
[18] E. Urnukhsaikhan, B. E. Bold, A. Gunbileg, N. Sukhbaatar and T. Mishig-Ochir, *Sci. Rep.*, **11**, 21047 (2021), https://doi.org/10.1038/s41598-021-00520-2
[19] Z. Shi, J. Tang, L. Chen, C. Yan, S. Tanvir *et al.*, *J. Mater. Chem. B*, **3**, 603 (2015), https://doi.org/10.1039/C4TB01647E
[20] R. Berker Demiral, O. Çağlar Kurtuluş and S. Ondaral, *Cellulose Chem. Technol.*, **59**, 237 (2025), https://doi.org/10.35812/CelluloseChemTechnol.2025.59.21
[21] O. Azougagh, S. Essayeh, N. Achalhi, A. El Idrissi, H. Amhamdi *et al.*, *Carbohyd. Polym.*, **276**, 118737 (2022), https://doi.org/10.1016/j.carbpol.2021.118737
[22] R. Chen, C. Yi, H. Wu and S. Guo, *Carbohyd. Polym.*, **81**, 188 (2010), https://doi.org/10.1016/j.carbpol.2010.02.012
[23] P. Kuppusamy, S. Kim, S.-J. Kim and K.-D. Song, *Arab. J. Chem.*, **15**, 104217 (2022), https://doi.org/10.1016/j.arabjc.2022.104217
[24] T. A. Le, Y. Guo, J. N. Zhou, J. Yan, H. Zhang *et al.*, *Int. J. Biol. Macromol.*, **194**, 110 (2022), https://doi.org/10.1016/j.ijbiomac.2021.11.180
[25] M. A. P. Morais, M. Silva, M. Barros, P. Halley, Y. Almeida *et al.*, *J. Appl. Polym. Sci.*, **141**, e56162 (2024), https://doi.org/10.1002/app.56162
[26] P. G. Seligra, C. Medina Jaramillo, L. Famá and S. Goyanes, *Carbohyd. Polym.*, **138**, 66 (2016), https://doi.org/10.1016/j.carbpol.2015.11.041
[27] K. V. Aleksanyan, E. E. Mastalygina, R. S. Smykovskaya, N. A. Samoilova, V. A. Novikov *et al.*, *Int. J. Mol. Sci.*, **26**, 10916 (2025), https://doi.org/10.3390/ijms262210916
[28] Y. Lan, Z. Xie, T. Wang, J. Lu, P. Li *et al.*, *Sustainability*, **15**, 9778 (2023), https://doi.org/10.3390/su15129778
[29] M. Hussain, T. Zahoor, S. Akhtar, A. Ismail and A. Hameed, *J. Food Sci. Technol.*, **55**, 1047 (2018), https://doi.org/10.1007/s13197-017-3018-5
[30] M. Ramos, E. Fortunati, M. Peltzer, F. Dominici, A. Jiménez *et al.*, *Polym. Degrad. Stab.*, **108**, 158 (2014), https://doi.org/10.1016/j.polymdegradstab.2014.02.011
[31] C. Demitri, R. Del Sole, F. Scalera, A. Sannino, G. Vasapollo *et al.*, *J. Appl. Polym. Sci.*, **110**, 2453 (2008), https://doi.org/10.1002/app.28660
[32] J. Sahoo, S. Sarkhel, N. Mukherjee and A. Jaiswal, *ACS Omega*, **7**, 45962 (2022), https://doi.org/10.1021/acsomega.2c06211
[33] L. Biao, S. Tan, Y. Wang, X. Guo, Y. Fu *et al.*, *Mater. Sci. Eng. C*, **76**, 73 (2017), https://doi.org/10.1016/j.msec.2017.02.154
[34] M. J. Hajipour, K. M. Fromm, A. A. Ashkarran, D. Jimenez de Aberasturi, I. R. de Larramendi *et al.*, *Trends Biotechnol.*, **30**, 499 (2012), https://doi.org/10.1016/j.tibtech.2012.06.004
[35] P. Bélteky, A. Rónavári, N. Igaz, B. Szerencsés, I. Y. Tóth *et al.*, *Int. J. Nanomed.*, **14**, 667 (2019), https://doi.org/10.2147/IJN.S185965
[36] A. Carrapiço, M. Pico, E. P. Carreiro, P. Barrulas, J. Mirão *et al.*, *Int. Biodeterior. Biodegrad.*, **205**, 106167 (2025), https://doi.org/10.1016/j.ibiod.2025.106167